Astron. Astrophys. 350, 423–433 (1999)

ASTRONOMY AND ASTROPHYSICS

Magnetic arms in NGC 6946 generated by a turbulent dynamo

R. Rohde[1], **R. Beck**[2], **and D. Elstner**[1]

[1] Astrophysikalisches Institut Potsdam, An der Sternwarte 16, 14482 Potsdam, Germany
[2] Max-Planck-Institut für Radioastronomie, Auf dem Hügel 69, 53121 Bonn, Germany

Received 1 June 1999 / Accepted 26 August 1999

Abstract. Dynamo models for the structure of the regular magnetic field in the galaxy NGC 6946 are confronted with recent observations of polarized radio emission at $\lambda 3.5$ cm. The observed behaviour of the concentration of regular fields *between* the gaseous spiral arms ("magnetic spiral arms") is achieved via a non-axisymmetric azimuthal distribution of only the correlation time $\tau_{\rm corr}$ of interstellar turbulence, determined by the typical size of interstellar clouds or the lifetime of supernova remnants or superbubbles. There is no need for the turbulent gas velocity of gas clouds to vary between arm and interarm regions. Furthermore, a satisfactory agreement between model and observations of the radial distribution of the regular field strength requires that the galaxy rotates differentially at radii beyond a few 100 pc, as indicated by observations of the molecular gas. Our model also explains the strong concentration of regular fields within the inner 2 kpc as well as the observed arm/interarm variation of the field pitch angle.

Key words: Magnetohydrodynamics (MHD) – ISM: magnetic fields – galaxies: individual: – galaxies: ISM – galaxies: magnetic fields – galaxies: spiral

1. Introduction

The phenomenon of interarm magnetic fields ("magnetic arms"), first discovered in NGC 6946, has been discussed from several points of view. Beck & Hoernes (1996) mentioned four possible explanations – density waves, instabilities, magnetic reconnection, dynamo theory. Until now some progress was achieved. Fan & Lou (1996) and Lou & Fan (1998) discussed the possibility that interarm magnetic fields are due to slow MHD density waves. However, such waves may exist only in the rigidly rotating part of a galaxy. Other attempts involved dynamo theory in the framework of a mean-field approach. Recent numerical simulations of a 3D nonlinear galactic dynamo concerned with interarm magnetic fields were investigated by Rohde & Elstner (1998) where the excitation of magnetic fields between the optical spiral arms was due to an enhanced turbulence intensity (and density) within the arms. Schreiber & Schmitt (1999) discussed a 3D linear galactic dynamo also achieving enhanced interarm magnetic fields since the α effect, the turbulent diffusivity and the large-scale velocity are all modulated by a stationary density wave. The occurrence of interarm magnetic fields in terms of dynamo numbers that describe the interplay between field inducing effects (differential rotation, α-effect and diffusivity) was discussed by Shukurov (1998) and Shukurov & Sokoloff (1998) for models with density and turbulence intensity both enhanced in the optical arms. With a 2D approximation Moss (1998) investigated nonlinear dynamos with spiral arms that are introduced via large-scale non-axisymmetric gas velocities, non-axisymmetric turbulent diffusivity and non-axisymmetric α-effect, respectively. All models show magnetic arms in interarm regions under the assumption of enhanced turbulent velocity in the optical arms. However, no observational hints were found yet in support of this assumption (see Sect. 4.2).

In the present investigation we try to get further insight into the magnetic field structure of NGC 6946 assuming that the field is generated by a nonlinear turbulent dynamo as introduced by Rohde & Elstner (1998). The excited magnetic field is discussed with respect to several properties of NGC 6946 as the distribution of gas density and turbulence intensity, rotation curve, corotation radius and spiral arm shape.

2. Observations

NGC 6946 is a typical late-type, gas-rich spiral galaxy. Distance measurements range between 5 and 10 Mpc; we assume 7 Mpc throughout this paper. NGC 6946 reveals a multiple-arm spiral structure in all spectral ranges (optical, infrared, far-infrared and radio continuum). Lacking a pronounced central bar and a companion galaxy, density waves are only of modest strength. The distribution of neutral hydrogen gas is quite smooth out to $\simeq 8$ kpc from the center (Boulanger & Viallefond 1992), and even molecular gas shows only a moderate arm/interarm contrast (Clausset et al. 1991).

Early radio polarization observations with low spatial resolution showed that the regular magnetic field of NGC 6946 is of spiral shape, similar to that of the optical spiral pattern (Harnett et al. 1989). Faraday rotation data indicated that NGC 6946 has an axisymmetric field (Ehle & Beck 1993). With increased resolution, however, the regular field appeared to be concen-

Send offprint requests to: R. Rohde (rrohde@aip.de)

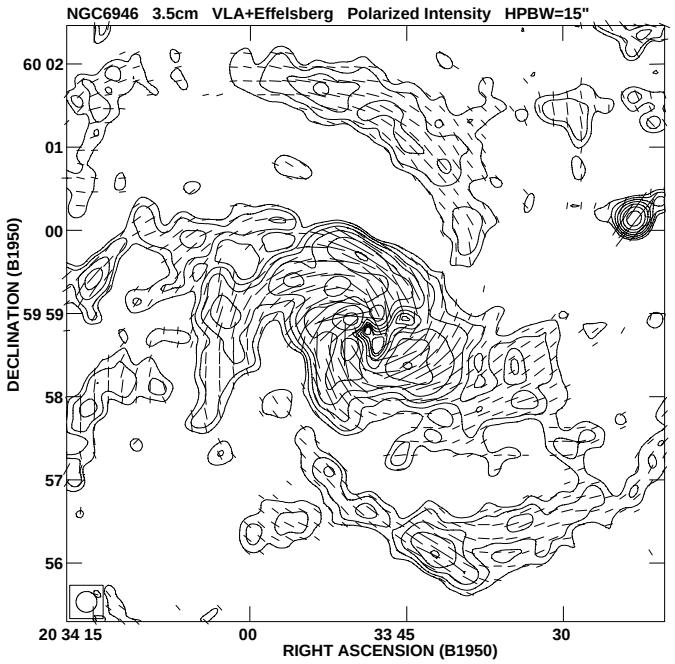

Fig. 1. Linearly polarized radio intensity of NGC 6946 at λ3.5 cm, combined from observations at the VLA and Effelsberg radio telescopes (Beck, in prep.). Contour levels are (1, 1.4, 2, 2.8, 4, 5.6, 8, 11, 16)$\times$40 μJy/beam. The length of the B-vectors is proportional to the polarized intensity. The angular resolution of 15″ is shown in the bottom left corner

trated in two "magnetic arms" *between* the optical arms (Beck & Hoernes 1996), inconsistent with axisymmetry. Faraday rotation measures indicate a mixture of axisymmetric ($m = 0$) and $m = 2$ modes, with the field direction pointing inwards everywhere (Krause & Beck 1998).

Fig. 1 shows a new polarization map at λ3.5 cm from observations of the 100-m Effelsberg radio telescope of the MPIfR and the VLA synthesis telescope of the NRAO.[1] At this wavelength, Faraday rotation is smaller than a few degrees and Faraday depolarization is negligible (Ehle & Beck 1993) so that Fig. 1 shows directly the orientation of the magnetic field. Details of the λ3.5 cm observations will be given elsewhere (Beck, in prep.)

Note that the *total* radio continuum emission, signature of the *total* magnetic field, is at any wavelength distributed similar to the optical and infrared emission, with its strongest intensities *on* the gaseous spiral arms.

3. Mean-field electrodynamics

The evolution of the mean regular magnetic field $\bar{\boldsymbol{B}}$ is governed by the dynamo equation

$$\frac{\partial \bar{\boldsymbol{B}}}{\partial t} = \mathrm{rot}\,(\bar{\boldsymbol{u}} \times \bar{\boldsymbol{B}} + \boldsymbol{\mathcal{E}}), \tag{1}$$

[1] The National Radio Astronomy Observatory is a facility of the National Science Foundation operated under cooperative agreement by Associated Universities, Inc.

where $\boldsymbol{\mathcal{E}}$ is the turbulent electromotive force (EMF), $\boldsymbol{\mathcal{E}} = \langle \boldsymbol{u}' \times \boldsymbol{B}' \rangle$ with $\boldsymbol{u}'$ the turbulence velocity and $\boldsymbol{B}'$ the turbulent magnetic field, and $\bar{\boldsymbol{u}} = (0,\, u_\phi,\, 0)$ the mean velocity of the differentially rotating interstellar gas (Krause & Rädler 1980).

As usual, we assume approximate scale separation and write

$$\mathcal{E}_i = \alpha_{ij} \bar{B}_k + \eta_{ijk} \bar{B}_{j,k}. \tag{2}$$

For the EMF we adopt here the concept used in the more general frame by Rohde & Elstner (1998). The α-tensor takes the form

$$\alpha_{ij} = \begin{pmatrix} \alpha_{rr} & -(U_z^{\rm dia} + U_z^{\rm buo}) & (U_\phi^{\rm dia} + U_\phi^{\rm buo}) \\ (U_z^{\rm dia} + U_z^{\rm buo}) & \alpha_{\phi\phi} & -(U_r^{\rm dia} + U_r^{\rm buo}) \\ -(U_\phi^{\rm dia} + U_\phi^{\rm buo}) & (U_r^{\rm dia} + U_r^{\rm buo}) & \alpha_{zz} \end{pmatrix} \tag{3}$$

with the diagonal terms

$$\alpha_{rr} = \alpha_{\phi\phi} = -\frac{4}{5}\tau_{\rm corr}^2 \Omega \tilde{\Psi} \left(u_{\rm T}^2 \frac{\partial}{\partial z} \log \rho + \frac{1}{3} \frac{\partial}{\partial z} u_{\rm T}^2 \right), \tag{4}$$

$$\alpha_{zz} = \frac{4}{5}\tau_{\rm corr}^2 \Omega \tilde{\Psi}_z \left(\frac{1}{3} u_{\rm T}^2 \frac{\partial}{\partial z} \log \rho + \frac{2}{3} \frac{\partial}{\partial z} u_{\rm T}^2 \right), \tag{5}$$

turbulent diamagnetism

$$\boldsymbol{U}^{\rm dia} = -\frac{c_\eta}{2} \Psi_{\rm dia} \tau_{\rm corr} \nabla u_{\rm T}^2 \tag{6}$$

and magnetic buoyancy

$$\boldsymbol{U}^{\rm buo} = u_{\rm T}^2 \Psi_{\rm buo} \tau_{\rm corr} \nabla \log \rho. \tag{7}$$

We introduced here the turbulence intensity (rms velocity)

$$u_{\rm T} = \sqrt{\langle \boldsymbol{u}'^2 \rangle}. \tag{8}$$

The angular velocity Ω is given via Eq. (11); the density distribution ρ is described in Sect. 4.3. The different quenching functions ($\tilde{\Psi}$, $\tilde{\Psi}_z$, $\Psi_{\rm buo}$, $\Psi_{\rm dia}$) represent the influence of the magnetic field strength β onto the turbulence effects. They are discussed in detail by Kitchatinov & Rüdiger (1992), Rüdiger & Kitchatinov (1993) and also by Elstner et al. (1996). The field strength β is normalized as $\beta = |\bar{\boldsymbol{B}}|/B_{\rm eq}$ with the equipartition field

$$B_{\rm eq} = \sqrt{\mu_0 \rho u_{\rm T}^2}. \tag{9}$$

(where μ_0 is the permeability, 4π in the cgs-system).

The scalar field $\eta_{\rm T}$ is given as

$$\eta_{\rm T} = c_\eta u_{\rm T}^2 \tau_{\rm corr} \tag{10}$$

with c_η = 0.3 (cf. Ruzmaikin et al. 1988). The feedback of the magnetic field onto the eddy diffusivity (Kitchatinov et al. 1994), which is not taken into account here, should be investigated in a future work.

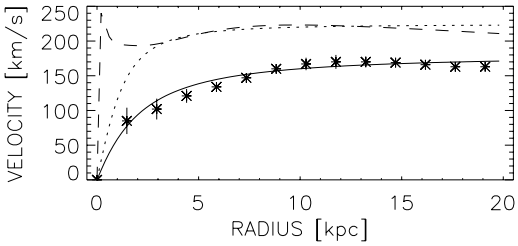

Fig. 2. Rotation velocities given by Carignan et al. (1990) (stars, with error bars) and by Sofue (1996) (dashed). Approximations used for our simulations are also shown (solid and dotted, respectively)

4. The model for NGC 6946

We consider galaxies to be differentially rotating turbulent disks embedded in a plasma of given conductivity (Elstner et al. 1990). In the simplest case the "plasma" is vacuum and the conductivity therefore vanishes. Thickness and height of the galactic disk are determined by the density scales, see Sect. 4.3. The calculated volume is restricted to the radius R = 15 kpc and the half-thickness H = 1.5 kpc. The simulations are performed with a 3D time-stepping code using cylindrical polar coordinates with a resolution of 41 gridpoints in each direction. The code is described in more detail in Elstner et al. (1990) and Rohde et al. (1998a). All calculations shown here are performed with an initial magnetic field composed of modes m=0,1 and a mixed parity with respect to the equatorial plane, but our tests have shown that the resulting magnetic field is independent of the initial field.

4.1. Differential rotation

We describe the differentially rotating gas by a Brandt-type law

$$u_\phi = r\Omega = r\Omega_0 \left(1 + \left(\frac{r}{r_\Omega}\right)^n\right)^{-1/n}. \qquad (11)$$

By selecting the values Ω_0 = 72 Gyr^{-1}, r_Ω = 2.5 kpc and n = 1.3 we approximate the rotation curve given in Carignan et al. (1990) on the basis of neutral hydrogen (HI) data. The asymptotic velocity reaches a value of $V_\infty = r_\Omega\Omega_0$ = 180 km s^{-1}. Our modeled rotation curve is shown in Fig. 2 (solid line).

The shape of rotation curves is still a topic of investigation. Sofue (1996) claimed that HI data compared to observations of the molecular gas (CO) yield too small velocity values, especially at small radii. An approximation to his (CO+HI) rotation curve for NGC 6946 is also shown in Fig. 2 (dashed line). For this rotation curve we choose the parameters Ω_0 = 220 Gyr^{-1}, r_Ω = 1 kpc and n = 2. In Sect. 5.5 we discuss the influence of the different rotation curves onto the magnetic field generation.

4.2. Non-axisymmetry

Since investigations of the H_2 and HI surface densities in the galaxy NGC 6946 have revealed that there are rather weak azimuthal variations of gas density (Tacconi & Young 1990; Boulanger & Viallefond 1992), we assume an axisymmetric density distribution for our galaxy model. Note that the influence of a non-axisymmetric density distribution onto the dynamo-induced magnetic field is very small and is thus neglected (Rohde & Elstner 1998).

The turbulence intensity u_T can be measured in principle by the velocity dispersion of spectral lines, e.g. HI (Boulanger & Viallefond 1992). However, other effects like unresolved velocity gradients or vertical gas motions will also increase the observed velocity dispersion. On the other hand, a strong arm/interarm contrast in turbulence intensity, as assumed in several previous papers (Shukurov 1998; Rohde & Elstner 1998; Moss 1998; Schreiber & Schmitt 1999) should be detectable through a significant difference in line widths. No such effect has been found in any galaxy so far. In particular, HI data for NGC 6946 do not show any difference in linewidth between arm and interarm regions near the minor axis (Kamphuis 1993 and Kamphuis, priv.comm.). Consequently, u_T is also assumed to be axisymmetric in our models.

We introduce a spiral profile attached *to only the correlation time* τ_corr of interstellar turbulence, whose value we take as a free parameter since it is indeed unknown. We assume that the correlation time is enlarged within the optical spiral arms of the galaxy. This configuration seems justified by the fact that small molecular clouds collide to form giant clouds in the arms and thus are larger than in the interarm regions (Casoli 1991). Assuming constant turbulence intensity u_T, larger molecular clouds are then correlated with enhanced correlation length and correlation time τ_corr.

The arm/interarm contrast is described via the shape of a logarithmic spiral

$$\mathcal{Q} = 1 + \frac{q-1}{2}\Big[1 + \cos\Big(2(\phi - \Omega_\mathrm{p}t) + 2\log\frac{r}{R}\cot\chi_\mathrm{opt}\Big)\Big], \qquad (12)$$

varying between 1 and q. The pitch angle χ_opt of the optical spiral arms was set to $-28°$ following Kennicutt (1981). The real spiral shape of NGC 6946 is of course more complicated than in our model (Elmegreen et al. 1992). On a red-light image Frick et al. (1999) identified four main spiral arms with average pitch angles between $-17°$ and $-37°$. In Sect. 5.3 we discuss the influence of different (optical arm) pitch angles χ_opt onto the magnetic field in order to justify our simplification.

4.3. Vertical stratification and radial scale lengths

Lacking knowledge about the vertical stratification of the gas density in NGC 6946 we adopt the empirical HI distribution of Dickey & Lockmann (1990) for our Galaxy: a combination of two Gaussians with central densities 0.395 and 0.107 cm^{-3} and scale heights of 212 and 530 pc, respectively, and an exponential with central density 0.064 cm^{-3} and a scale height of 403 pc. We add a further Gaussian with mid-plane density 0.3 H_2 cm^{-3} and half-width 70 pc to include the molecular gas layer (cf. Bloemen 1987), and an exponential with a scale height of 1.5 kpc and a mid-plane density of 0.025 cm^{-3} representing the extended ionized gas (Reynolds 1989). The total gas mass of NGC 6946

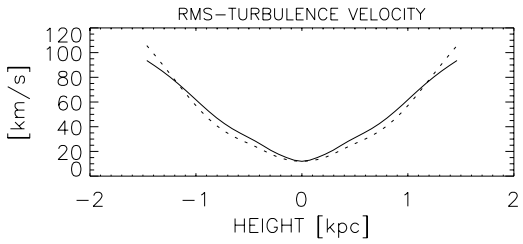

Fig. 3. The maximal turbulence intensity (rms turbulence velocity) calculated from Eq. (13) at radius r = 3.75 kpc (solid) and r = 11.25 kpc (dashed)

is approximately twice that of our own Galaxy (Carignan et al. 1990). Note that the total gas mass does not influence the vertical stratification (Eq. (13)). It only determines the equipartition field strength $B_{\rm eq}$ and therefore the strength of the magnetic field that saturates the dynamo by α-quenching, but has no influence onto the field structure.

We further introduce exponential scale lengths for the different components of the gas disk of NGC 6946 (Tacconi & Young 1986): 10 kpc (HI), 3.5 kpc (HII) and 3 kpc (H_2).

Based on the given density stratification we adopt the common simplification of the vertical momentum equation as a possibility to calculate the turbulence intensity:

$$\gamma \frac{d}{dz}\left(\rho(z) u_{\rm T}^2(z)\right) = -\rho(z) k_z \qquad (13)$$

The used potential k_z is essentially due to a self-gravitating isothermal sheet of stars with constant thickness z_0 and we assume

$$k_z(z) = \frac{2\sigma^2}{z_0} \tanh\left(\frac{z}{z_0}\right). \qquad (14)$$

Lacking knowledge on the exact density distribution in NGC 6946 and for the sake of simplicity we neglect radial dependencies within the potential k_z. We set an average value σ = 21.5 km s^{-1} for the vertical velocity dispersion of the old disk stars and z_0 = 0.6 kpc. The value for γ should be larger than 1 (Elstner et al. 1996); here we assume γ = 3 (see Fröhlich & Schultz (1996) and Elstner et al. (1996) for details).

The velocity dispersion in HI shows a radial dependency decreasing outwards from approximately 16 km s^{-1} to 8 km s^{-1} (Boulanger & Viallefond, 1992). This may be interpreted as a radial decrease of the turbulent gas velocity, but there may be other reasons (see Sect. 4.2). In our 'standard' model we assume a constant mid-plane turbulence intensity with an average value of $u_{\rm T}(z = 0)$ = 12 km s^{-1}, in Sect. 5.4 we also investigate a model with radially decreasing mid-plane turbulence intensity. Note that below and above the galactic mid-plane the turbulence intensity slightly depends on r because the galactic density decreases outwards (cf. Fig. 3 and Eq. (13)).

5. Results

5.1. 'Standard' model for NGC 6946

As a main result we achieve a basically axisymmetric magnetic field (ASS) with a clear maximum of the strength of the regular field within the interarm regions (Fig. 4, Fig. 5a). The field is strongest at $\simeq$ 3 kpc radius (Fig. 6). The magnetic field mode m = 2 is given preference by the two-armed profile in $\tau_{\rm corr}$ and reaches almost 20% of the magnetic energy density (Fig. 8). The general structure of the simulated magnetic field is in agreement with the models based on small correlation times shown in Rohde & Elstner (1998): the field is strongly determined by the effect of differential rotation. Within our model, the relatively high mid-plane turbulence intensity ($u_{\rm T}(z = 0)$ = 12 km s^{-1}) requires a relatively small correlation time of interstellar turbulence, otherwise the turbulent dynamo would lead to magnetic pitch angles which are too large compared to the observations, or the dynamo would change to the α^2-regime. For the model presented in this section we use values $\tau_{\rm corr}$ of 0.01 Gyr (interarm) to 0.02 Gyr (arm), comparable to the lifetime (merging time) of supernova remnants and of giant molecular clouds. Ferrière (1998) mentions merging times for superbubbles in the range 0.01 to 0.04 Gyr.

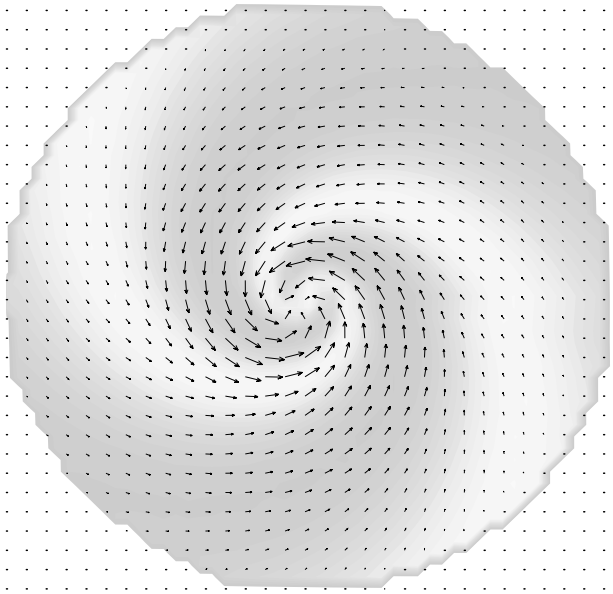

Fig. 4. Magnetic field geometry in the galactic mid-plane for an azimuthal variation of $\tau_{\rm corr}$ = 0.01 ... 0.02 Gyr. The optical spiral arms (enlarged $\tau_{\rm corr}$) are shown by light shades.

The magnetic pitch angle reaches values between $-17°$ ("magnetic arms") and $-38°$ ("magnetic interarm" = gaseous arms) (Fig. 5b) and thus varies by about $\pm 10°$ around the pitch angle of the gaseous arms in our models (assumed to be constant). Fig. 7 shows the mean value of the magnetic pitch angle taken in the galactic mid-plane averaged over all azimuthal angles.

5.2. Role of the corotation radius

The corotation radius of the spiral pattern and the interstellar gas influences the geometry of the magnetic field. For radii smaller than $r_{\rm co}$ the region with maximal magnetic field is shifted towards the spiral arm preceding in the sense of rotation (with

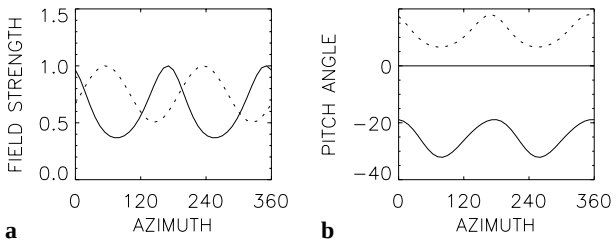

Fig. 5a and b. $\bar{B}^4$, where $\bar{B}$ is the normalized regular magnetic field strength (solid) compared with the profile in correlation time (dotted, also normalized) **a**. The field shows a concentration between the gaseous spiral arms. We show $\bar{B}^4$ to allow a comparison with the polarized intensity (Sect. 6.3). **b** Magnetic pitch angle (solid) compared with the normalized magnetic field strength (dotted). The absolute value of the magnetic pitch angle is largest between the "magnetic arms", i.e. in the gaseous (optical) arms. Both plots are given for the galactic mid-plane at r = 6 kpc

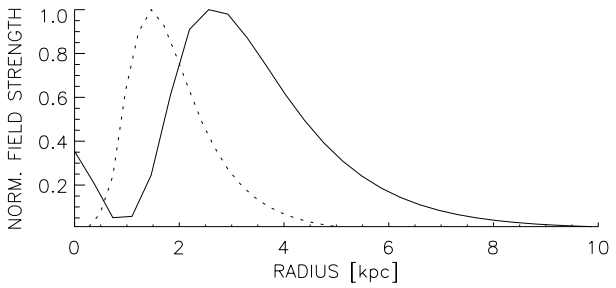

Fig. 6. $\bar{B}^4$ (normalized) for the 'standard' model (solid) and a model based on the rotation curve given by Sofue (1996) (dotted) in the galactic mid-plane, averaged over all azimuthal angles

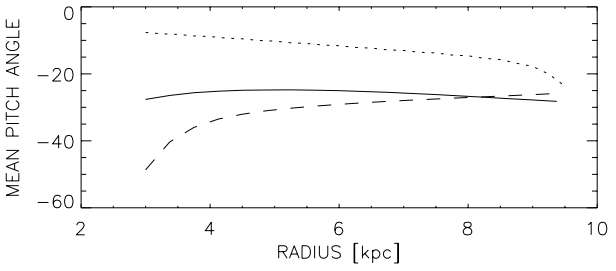

Fig. 7. Mean magnetic pitch angle in the galactic mid-plane averaged over all azimuthal angles for the 'standard' model (solid), for the model with outward-decreasing turbulence intensity (dashed) (see Sect. 5.4) and for the model based on the rotation curve given by Sofue (1996) (dotted) (see Sect. 5.5)

enhanced correlation time); outside corotation radius the field is shifted towards the following arm (Fig. 9). Hence, a shift of 90° occurs at the corotation radius.

This phenomenon is expected to be due to the fact that the interstellar gas rotates faster than the spiral pattern for radii smaller than $r_{\rm co}$. The partially frozen-in magnetic field lines are then transported by the gas from the interarm region towards the preceding arm. For radii larger than $r_{\rm co}$ the process works in the opposite manner. This explains the observed similarity between

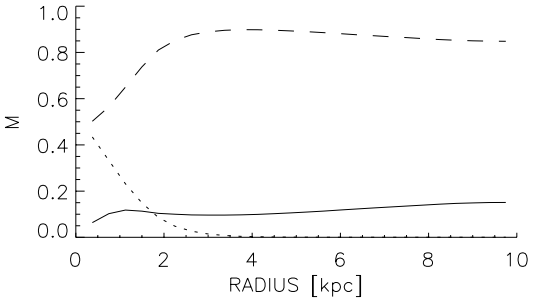

Fig. 8. Normalized contribution of the magnetic field energy ('standard' model) of mode m = 0 (dashed), 1 (dotted) and 2 (solid) at several radii. The m = 2 magnetic field contribution reaches values up to 20% of the magnetic energy density

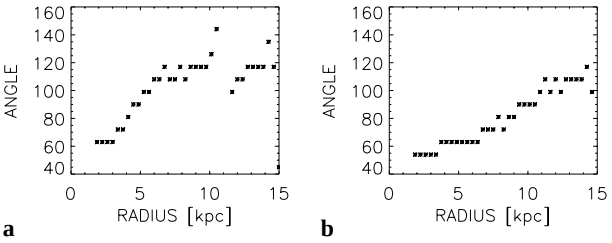

Fig. 9a and b. Phase shift between region of maximal magnetic field and the preceding spiral arm for a model with a corotation radius of $r_{\rm co}$ = 5 kpc **a** and 10 kpc **b**

the magnetic arms and their preceding optical arms (Frick et al. 1999) (see also Sect. 6.3).

According to Elmegreen et al. (1992) the corotation radius of NGC 6946 is located at about 2.6′ ($\simeq 5.2$ kpc at the distance assumed in this paper). The "magnetic arms" are observed between about 5 and 12 kpc radius (see Fig. 1) so that we would expect a phase shift with respect to the preceding arm of $90°$–$120°$. From the observational data, the mean shift is only between $\simeq 30°$ and $\simeq 70°$ for the four main arms (Frick et al. 1999, see also Sect. 6.3) which fits better to a large corotation radius (Fig. 9b). More detailed data of the galaxy's velocity field are required to determine the corotation radius with higher accuracy.

Note that a behaviour opposite to that in our models was found for the m = 1 mode excited by a spiral density wave (Mestel & Subramanian 1991, Subramanian & Mestel 1993), i.e. no phase shift between gas and magnetic field around the corotation radius. This is probably due to the neglection of α_{rr} and α_{zz} in their model (see Sect. 6.3). In our models, the m = 1 mode is unimportant unless the correlation time is very large, e.g. $\tau_{\rm corr} \approx 0.1$ Gyr (see Rohde & Elstner 1998).

5.3. Role of the spiral arm pitch angle

We further performed calculations with varied pitch angle $\chi_{\rm opt}$ of the gaseous arms and hence the turbulence profile (Eq. (12)).

The main and striking result is that the magnetic pitch angle $\varphi_{\rm m}$ is *only weakly* attached to the (optical arm) pitch angle $\chi_{\rm opt}$ of the underlying non-axisymmetric turbulence profile (Figs. 10,

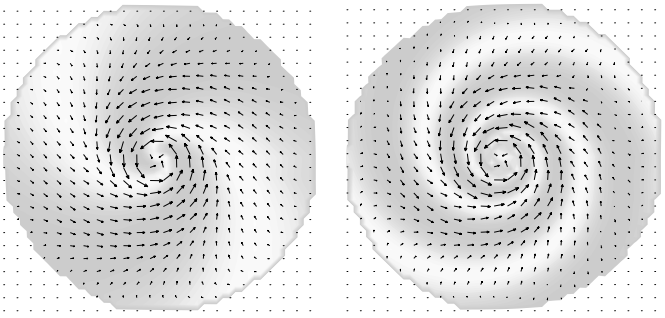

a **b**

Fig. 10a and b. Magnetic field geometry for different turbulence profiles in the galactic mid-plane. The optical spiral arms (enlarged $\tau_{\rm corr}$) with $\chi_{\rm opt}$ = 40° **a** and $\chi_{\rm opt}$ = 15° **b** are shown by light shades. The magnetic pitch angle does not depend on the galactic spiral profile, see also Fig. 11

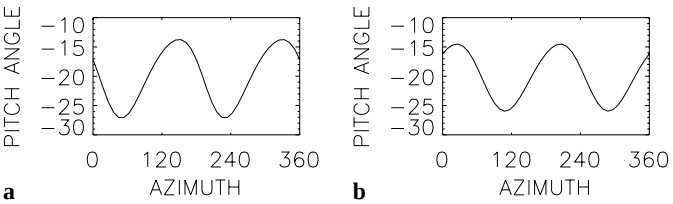

Fig. 11a and b. Magnetic pitch angle in the galactic mid-plane at $r = 1/3R$ for (optical arm) pitch angles $\chi_{\rm opt}$ = 40° **a** and $\chi_{\rm opt}$ = 15° **b** of the $\tau_{\rm corr}$-profile. The pitch angle of the $\tau_{\rm corr}$-profile shows almost no influence on the values of the magnetic pitch angle

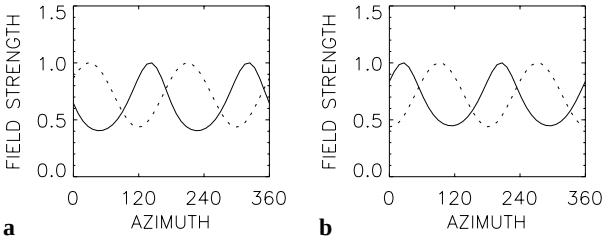

Fig. 12a and b. $\bar{\boldsymbol{B}}^4$ (normalized) (solid) compared with the turbulence profile $\tau_{\rm corr}$ (dotted, also normalized) in the galactic mid-plane at $r = 1/3R$ for (optical arm) pitch angles $\chi_{\rm opt}$ = 40° **a** and $\chi_{\rm opt}$ = 15° **b** of the $\tau_{\rm corr}$-profile. The regular field is always concentrated between the spiral arms

11) whereas the strength of the regular field is *always* highest in the interarm regions (Fig. 12). That is, the magnetic pitch angle and the field strength are generally determined by the turbulent diffusivity, the differential rotation and the values of the α-tensor, but not by the geometry of the optical spiral (see Sect. 4.2). This argumentation is of course only valid for an axially symmetric large-scale velocity field. Additional non-axisymmetric gas flows would strongly affect the magnetic field and its pitch angle (cf. Elstner et al. 1998).

We expect that a more complicated and more realistic spiral arm profile would not lead to qualitative different results.

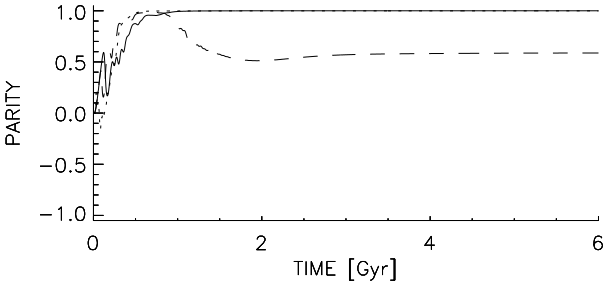

Fig. 13. Parity of the magnetic field for the 'standard' model (solid), for the model with outward-decreasing turbulence intensity (dashed) (see Sect. 5.4) and for the model based on the rotation curve given by Sofue (1996) (dotted) (see Sect. 5.5)

5.4. Radial decrease of mid-plane turbulence intensity?

The model we discussed in Sect. 5.1 is based on a mid-plane turbulence intensity that does not vary in radial (and azimuthal) direction. Since there are observations suggesting an outward-decreasing turbulence intensity profile (Boulanger & Viallefond 1992, see Sect. 4.3) we try to understand the consequences of such a profile by an appropriate simulation. We chose a slightly reduced decrease where the turbulence intensity in the galactic mid-plane varies linearly from 14 km s^{-1} in the center to 10 km s^{-1} at the outer radius (15 kpc).

Two main consequences appear being different to the 'standard' model presented in Sect. 5.1:

- The absolute value of the magnetic pitch angle now decreases in the outward direction, but it has also larger values at inner radii compared with the 'standard' model (Fig. 7).
- The magnetic field shows a considerable asymmetry with respect to the galactic mid-plane: The magnetic field modes A0 and A2 are excited besides the S0 and S2 modes. The asymmetry is well seen in a meridional plot of the azimuthal magnetic field ($\bar{\boldsymbol{B}}_\phi$) in Fig. 14b. This asymmetry leads to a strong vertical magnetic field ($\bar{\boldsymbol{B}}_z$) passing through the inner galactic disk without changing its sign which should be observable via strong Faraday rotation (Fig. 15) (see Sect. 6.4). The parity $P = E_{\rm S} - E_{\rm A}/(E_{\rm S} + E_{\rm A})$ of the magnetic field is shown in Fig. 13. The asymmetry mentioned above leads to a value of $P \simeq 0.5$ (dashed curve).

The behaviour of the magnetic pitch angle can be estimated by

$$\varphi_{\rm m} \approx -\sqrt{\frac{C_\alpha}{C_\Omega}} \tag{15}$$

(Beck et al. 1996). In the linear case, the approximations $\alpha \propto \tau_{\rm corr}^2 u_{\rm T}^2 \Omega/h$ and $\eta_{\rm T} \propto u_{\rm T}^2 \tau_{\rm corr}$ with the characteristic scale height h, inserted into the expressions of the induction coefficients

$$C_\alpha \propto \frac{\alpha h}{\eta_{\rm T}} \propto \tau_{\rm corr}\Omega, \qquad C_\Omega \propto \frac{\Omega h^2}{\eta_{\rm T}} \propto \frac{\Omega h^2}{u_{\rm T}^2 \tau_{\rm corr}} \tag{16}$$

give the estimation $\varphi_{\rm m} \approx -\sqrt{u_{\rm T}^2 \tau_{\rm corr}^2/h^2}$. In the nonlinear case (adopted here) a quenching function Ψ must be added in order to represent the influence of α-quenching. This gives

$$\varphi_{\rm m} \approx \sqrt{\frac{u_{\rm T}^2 \tau_{\rm corr}^2 \Psi}{h^2}}. \quad (17)$$

The quenching function, which in a simple estimation is $\Psi \propto 1/(1+\bar{\boldsymbol{B}}^2/B_{\rm eq}^2)$ (Beck et al. 1996), forces the absolute value of the magnetic pitch angle to increase outwards since the magnetic field is large around r_Ω and decreases outwards. This behaviour is well seen in the calculations shown in Fig. 7 (standard model) and Fig. 18. This effect is blurred in case of outward-decreasing turbulence intensity $u_{\rm T}$ where the absolute value of the magnetic pitch angle decreases outwards (Fig. 7, dashed).

Using the estimation (17) we can also explain the enlarged magnetic pitch angles within the the gaseous arms where the correlation time is assumed to be larger than in the magnetic arms.

Note that, according to Eq. (17), the same radial variation of the magnetic pitch angle occurs if one assumes a radial decrease of the correlation time e.g. because the mean size and/or lifetime of molecular clouds decreases outwards.

5.5. Role of the rotation curve

We discuss here how the field generation is influenced by the shape of the rotation curve. To avoid numerical problems due to the limited resolution of our simulations at the sharp increase of the velocity for $r < 1$ kpc, we approximate the rotation curve by Sofue (1996) using a Brandt-type law with Ω_0 = 220 Gyr^{-1}, r_Ω = 1 kpc and n = 2 (Fig. 2). The shape of the spiral arms and the distributions of density, turbulence intensity and correlation time are the same as for our 'standard' model discussed in Sect. 5.1.

The investigation of Sofue's rotation curve leads to a magnetic field with rather small absolute values of the magnetic pitch angle due to the stronger differential rotation (Fig. 7, dotted). The magnetic field is more concentrated at inner radii (Fig. 6). The contribution of higher magnetic field modes (m =2) and thus the influence of the spiral arms is smaller than in the 'standard' model. These field properties can be seen by comparing the magnetic fields of different models in the galactic mid-plane (Fig. 16).

Note that for very inner radii the approximation of the rotation curve given in Sofue (1996) is not very accurate. Therefore we expect that, for a better approximation of the sharp velocity increase, the above mentioned differences to the 'standard' model would be even larger.

6. Discussion

We confront our models with the radio polarization observations at λ3.5 cm (Fig. 1) which are almost free from Faraday effects.

6.1. Radial variation of the polarized intensity

The observed polarized synchrotron intensity is concentrated in the central region and decreases strongly within a few kpc from the center (Fig. 17). If the density of cosmic-ray electrons is constant, the total synchrotron intensity scales roughly with B_{tot}^2 and the polarized intensity with $\bar{\boldsymbol{B}}^2$ (see Beck et al. 1996 for details), where B_{tot} and $\bar{\boldsymbol{B}}$ are the strengths of the total and regular fields, respectively. In this case, none of our models can explain the strong central concentration of the polarized emission. If, on the other hand, the energy density of cosmic rays is in equipartition with the magnetic energy density, the scaling is $\bar{\boldsymbol{B}}^4$ and our models predict a strong radial decrease of polarized intensity. However, the distribution in our 'standard model' (Fig. 6) is still too broad. To achieve a sufficiently narrow concentration of $\bar{\boldsymbol{B}}^4$, we need differential rotation of NGC 6946 from a few 100 pc radius until the outer galactic disk, as in the rotation curve by Sofue (1996) (see Fig. 2).

In the rotation curve by Carignan et al. (1990) differential rotation is so small within the inner kpc that the α-Ω dynamo cannot operate. For strong dynamo excitation an α^2 dynamo is still possible, but no magnetic arms between the optical arms are expected in this regime (see Rohde & Elstner 1998). More velocity data, e.g. in CO lines, are required to obtain an accurate rotation curve.

At inner radii ($r < 1$ kpc) our models show a minimum of the magnetic field strength, inconsistent with the observations (Fig. 17). The reason is the insufficient approximation of Sofue's rotation curve in the very central region (Fig. 2). Dynamo models with increased spatial resolution in the inner region are necessary to achieve more realistic results at the very inner radii.

6.2. Radial variation of the magnetic pitch angle

Our 'standard' model reveals a radial increase of the absolute value of the magnetic pitch angle, averaged over all azimuthal angles (Fig. 7), while it slightly decreases in the model with outward-decreasing turbulence intensity, consistent with radio observations. Note that the main optical arms also become more tightly wound up in the outer regions of the galaxy (Frick et al. 1999).

The absolute values of the pitch angles in the preferred model using Sofue's rotation curve and the correlation times of the 'standard' model turn out to be too small. Increasing the correlation time leads to models with large-scale field reversals and therefore a ring-like structure. Such field configurations are especially a subject of discussion of the magnetic field in our Galaxy (cf. Indrani & Deshpande 1998), but they do not fit the situation observed in NGC 6946. To achieve reasonable agreement with the observations, we choose a model with enlarged turbulence intensity of 15 km s^{-1} in the galactic mid-plane. This value is larger than that given in Boulanger & Viallefond (1992), especially at larger radii (see Sect. 4.3). We do not have sufficient knowledge about the vertical stratification in NGC 6946. Thus we may expect that a more adequate profile in density will allow to avoid this inaccuracy in the mid-plane turbulence

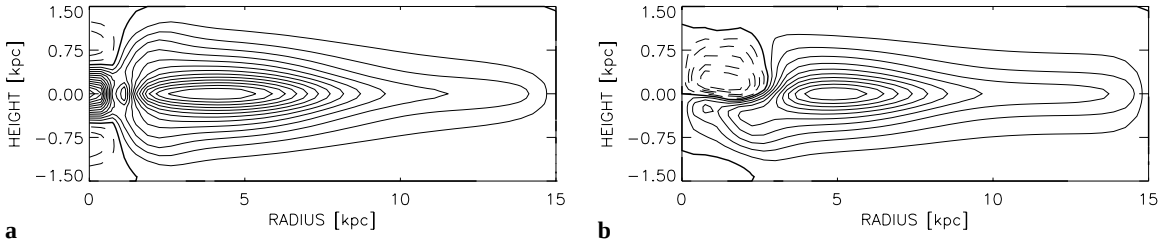

Fig. 14. **a** Meridional plot of the toroidal magnetic field ($\bar{\boldsymbol{B}}_\phi$) taken from the 'standard' model discussed in Sect. 5.1. The field is clearly symmetric with respect to the galactic mid-plane and shows a strong concentration there. **b** Meridional plot of the toroidal magnetic field ($\bar{\boldsymbol{B}}_\phi$) taken from the model with outward-decreasing turbulence intensity in the mid-plane (see Sect. 5.4). The field also contains antisymmetric components with respect to the mid-plane (A0, A2)

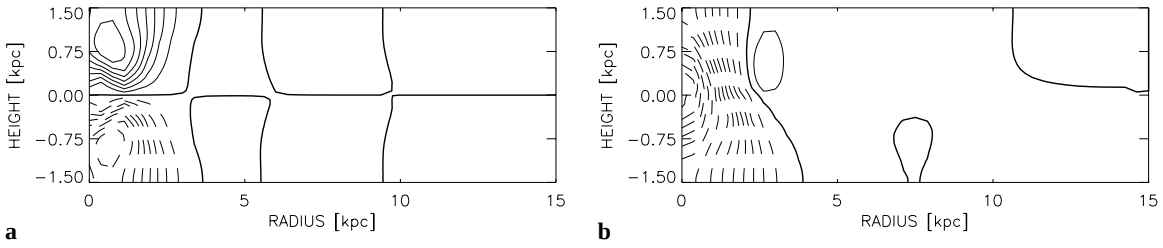

Fig. 15a and b. Meridional plot of vertical magnetic field component $\bar{\boldsymbol{B}}_z$ taken from the 'standard' model discussed in Sect. 5.1 **a** and from the model with outward-decreasing turbulence intensity **b**. In the latter case the vertical magnetic field passes through the inner galactic disk without changing sign due to the contribution of A-modes

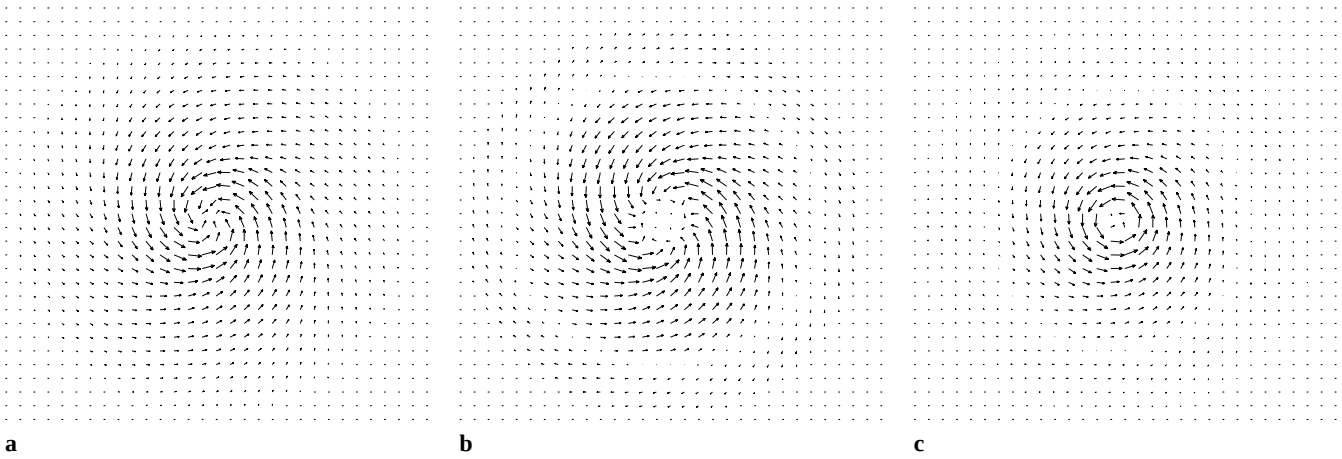

Fig. 16a–c. Magnetic field geometry taken in the galactic mid-plane. **a** For the 'standard' model discussed in Sect. 5.1 (cf. Fig. 4). **b** For a model with outwards decreasing turbulence intensity as discussed in Sect. 5.4. **c** For a model with a rotation curve based on Sofue (1996) as discussed in Sect. 5.5

intensity, since the density stratification affects the turbulence intensity (cf. Eq. (13)).

The turbulence intensity is assumed to be constant along radius because the model with outward-decreasing turbulence is in conflict with Faraday rotation data (see Sect. 6.4). The correlation times are again 0.02 Gyr (arm) and 0.01 Gyr (interarm). This defines our 'best model'.

However, our 'best model' with constant turbulence intensity is not completely satisfactory because it is unable to explain the observed radial variation of pitch angles (Fig. 18). At inner radii the achieved absolute values of the pitch angles are too small, whereas they tend to be too large for radii $r > 6$ kpc. With better observational data on the widths of spectral lines and cloud sizes, we hope to get refined values of turbulence intensity and/or correlation time and their radial variations as input parameters for improved models.

The magnetic pitch angle in our models is almost independent of the optical pitch angle (Sect. 5.3). The observed similarity between the magnetic and optical pitch angles may indicate some interplay between the spiral density wave and the dynamo wave. Preceding investigations (cf. Moss 1997 and references therein) dealt with the influence of a given non-axisymmetry onto the magnetic field, e.g. the influence of a density wave onto

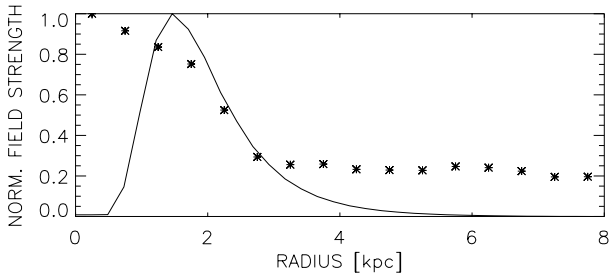

Fig. 17. Radial variation of the mean expected polarized intensity (represented by $\bar{\boldsymbol{B}}^4$ where $\bar{\boldsymbol{B}}$ is the mean strength of the regular field) in the galactic mid-plane for our 'best model', using Sofue's rotation curve (see Fig. 2), a radially constant turbulence intensity of 15 km s^{-1} and a correlation time of 0.02 Gyr (arm) and 0.01 Gyr (interarm). Observational data at $\lambda 3.5$ cm are given as stars; their errors are invisibly small

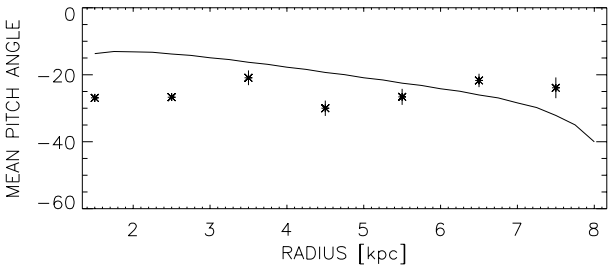

Fig. 18. Radial variation of the mean magnetic pitch angle in the galactic mid-plane for our 'best model', using Sofue's rotation curve (see Fig. 2), a radially constant turbulence intensity of 15 km s^{-1} and a correlation time of 0.02 Gyr (arm) and 0.01 Gyr (interarm). Observational data at $\lambda 3.5$ cm and their errors are given as stars

the dynamo wave (parametric resonance), but the behaviour of the magnetic pitch angle was not investigated.

On the other hand, the discussion of a back-reaction of the magnetic field onto the large-scale gas motion (e.g. the density wave) is still lacking because this back-reaction is neglected in the frame of present-day kinematic dynamo models. This simplification is generally justified by the weakness of galactic magnetic fields, i.e. the energy density of the magnetic field is small compared to the kinetic energy of the large-scale motion of the interstellar gas. This assumption is possibly not true in the magnetic arms since the strength of the regular field is enhanced there Both energy densities are comparable for $\bar{\boldsymbol{B}} \simeq 10$ μG and $\rho \simeq 0.02$ cm^{-3} (assuming $u_\varphi \simeq 150$ km s^{-1}) (Beck & Hoernes 1996). The gas density there is still unknown because deep CO observations are not available. A further nonlinear effect that should be taken into account in future models is the back-reaction of the magnetic field onto the turbulent diffusivity (η-quenching) (cf. Elstner et al. 1996; Rohde et al. 1998a; Moss 1998).

6.3. Azimuthal variations of the field

Fig. 19 shows the azimuthal variations of $\bar{\boldsymbol{B}}^4$ and the magnetic pitch angle of our 'best model' which are both in reasonable agreement with the observational data. The strongly deviating pitch angles at $140^\circ - 150^\circ$ azimuth correspond to the kink in the magnetic arm in the south ($RA \simeq 20^h33^m38^s$, $DEC \simeq 59^\circ56'$, see Fig. 1). The optical arm in the southeast ($\simeq 70^\circ$ ahead in azimuth) shows a similar kink.

Our models predict that the absolute values of the pitch angle should be larger in the gaseous arms than in the magnetic arms (Fig. 5). The gaseous arms coincide with the arms of total radio emission where the magnetic field is strongest, but mostly irregular (Beck & Hoernes 1996). In the ring between 5 and 7 kpc radius two broad arms can be identified, located at 0°–80° and 200°–250° azimuthal angle. These regions are those with the largest absolute values of the pitch angle (Fig. 19b). However, the errors are large due to the low polarized intensity in the gaseous arms. Future polarization observations with higher resolution may partly resolve the field structure so that the detectable polarized intensity might become higher.

The phase shift between the magnetic and the preceding gaseous arms is predicted to increase with radius (Fig. 9b), from $\simeq 65^\circ$ at 5 kpc to $\simeq 90^\circ$ at 10 kpc radius (corotation). Frick et al. (1999) found that the phase shifts as determined from the radio polarization and red-light images are roughly constant. Taking into account the observational errors, this result agrees with our model.

It is remarkable that the concentration of regular magnetic field between the gaseous spiral arms in our models is only caused by the non-axisymmetric distribution of correlation time $\tau_{\rm corr}$, whereas in all previous papers this effect was achieved via modulation of the turbulence intensity (Rohde & Elstner 1998; Shukurov 1998; Moss 1998; Schreiber & Schmitt 1999). The pronounced "magnetic arms" in the interarm regions are due to the interplay of α^2 and α-Ω induction processes and are only weakly influenced by the nonlinear back-reaction on the turbulence. This is why the process is also working for uniform turbulence intensity, contrary to earlier concepts. In Rohde et al. (1998b) we estimated a local dynamo number

$$D \propto |C_\alpha \left(C_\alpha - C_\Omega\right)| \propto \left|\Omega^2 \Psi \left(\tau_{\rm corr}^2 \Psi - \frac{h^2}{u_{\rm T}^2}\right)\right| \qquad (18)$$

reflecting the interplay between the two interfering induction processes described by C_α and C_Ω (cf. Eq. (16)). (The quenching function Ψ is introduced via α-quenching, see Sect. 5.4.) Due to the rather small values of the correlation time our models for NGC 6946 work in the α-Ω regime. In this case the induction is dominated by the C_Ω induction coefficient within the dynamo number (Eq. (18)). *Increasing* $\tau_{\rm corr}$ in the optical arms then *decreases* the dynamo number in this region: The field generation works preferably in the interarm region. (Remember that the turbulence intensity $u_{\rm T}$ has no arm/interarm contrast in our models.) The back-reaction of the magnetic field onto the turbulence (α-quenching) cannot explain the existence of magnetic arms: As the equipartition field $B_{\rm eq}$ (Eq. (9)) is axisymmetric in our models but the regular field $\bar{\boldsymbol{B}}$ is stronger in the magnetic arms, α-quenching suppresses the formation of such arms. Our models indicate that the effect of higher local dynamo numbers in the interarm regions is more important.

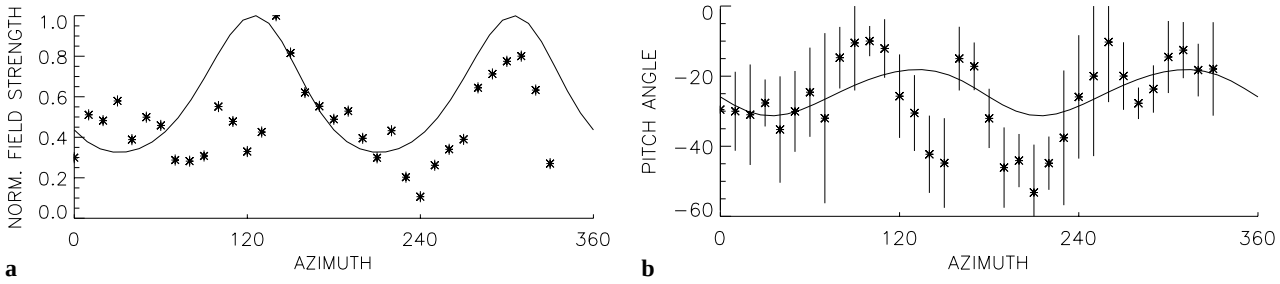

Fig. 19a and b. Azimuthal variation of the expected polarized intensity ($\bar{B}^4$) **a** and of the magnetic pitch angle **b** of our 'best model', both at a radius of 6 kpc. The turbulence intensity is 15 km s^{-1} (mid-plane value), the correlation time varied between 0.02 Gyr (arm) and 0.01 Gyr (interarm). Observational data (averaged between 5 and 7 kpc radius) are given as stars. The azimuthal angle runs counterclockwise in the plane of the galaxy ($PA = 52^\circ$, $i = 30^\circ$), starting from the northeastern major axis

For a strong α-effect the second term in Eq. (18) could be neglected and an enhanced α (higher local dynamo number) in the arms leads to stronger magnetic fields in the optical arms with a bisymmetric structure. This was first noticed by Mestel & Subramanian 1991 and verified with a full 3D simulation by Rohde & Elstner (1998).

6.4. Faraday rotation

The large-scale distribution of Faraday rotation in NGC 6946 indicates that the field points towards us in the northeastern magnetic arm and away from us in the southwestern arm (Krause & Beck 1998). This is the typical signature of a mixture of $m = 0$ and $m = 2$ modes, in agreement with the models discussed in this paper.

No significant increase of Faraday rotation has been observed within the inner 2 kpc, as predicted by our model with outward-decreasing turbulence intensity (Fig. 15b). Consequently, our 'best model' assumes a constant turbulence intensity. This is not necessarily in conflict with the observed decrease of velocity dispersion (see Sect. 4.3) because other phenomena like unresolved velocity gradients or vertical gas motions affect the observed dispersion. Radio data in the HI and CO lines with better angular resolution are required.

7. Summary

We presented a theoretical model for the regular magnetic field in NGC 6946 based on the concept of a turbulent dynamo and we confronted our numerical results with present observations of polarized radio emission.

Our dynamo model assumes axisymmetric distributions of large-scale velocity, density contribution and turbulence intensity, because observations indicate only weak azimuthal variations. The optical spiral arms were introduced only via the correlation time of interstellar turbulence. The radial distribution of the gas density was also taken from observations. Since there is some discord in the literature about the rotation in NGC 6946 we investigated two possible rotation curves (Carignan et al. 1990; Sofue 1996). We further introduced a vertical stratification of the gas density and of the turbulence intensity. Without accurate knowledge about the distribution in NGC 6946 we assumed a stratification similar to that in our own Galaxy. Our dynamo model is nonlinear: We allowed the back-reaction of magnetic field onto the α-effect, but we neglected the influence onto the eddy diffusivity and on the large-scale gas motion.

Our basic results can be summarized as follows:

(i) *Rotation curve.* The observed narrow distribution of polarized radio intensity (cf. Fig. 17) is well reproduced by assuming equipartition between the cosmic-ray and magnetic field energy densities and a rotation curve similar to that one adopted by Sofue (1996). A model using the rotation curve of Carignan et al. (1990) leads to a too broad distribution of the regular magnetic field. However, our model fails within 1 kpc radius because the inner part of the observed rotation curve could not be modeled appropriately.

(ii) *Radial dependency of turbulence intensity.* There are some observational indications of an outward-decreasing turbulence intensity (Boulanger & Viallefond 1992). Although this decrease can reproduce the observed outwards decreasing absolute value of the magnetic pitch angle, it leads to considerable changes in the properties of the model (field reversals, strong vertical field components) which are in conflict with Faraday rotation data. For our 'best model' based on Sofue's rotation curve we chose a radially constant and rather large turbulence intensity (15 km s^{-1} mid-plane value) to achieve magnetic pitch angles of the right order (cf. Fig. 18). However, we were not able to reproduce its radial decrease satisfactorily.

(iii) *Spiral arms.* The basic property of the "magnetic arms" between the optical arms are well reproduced in our dynamo models (a result of superposition of magnetic field modes S0 and S2). The arm/interarm contrast in the polarized intensity and the corresponding values of the magnetic pitch angle $\varphi_{\rm m}$ in agreement with the observations are achieved by a contrast in *only* the correlation time of interstellar turbulence, varying between 0.02 Gyr (arm) and 0.01 Gyr (interarm) (cf. Fig. 19). The adopted pitch angle of the optical arms $\chi_{\rm opt}$ has almost no influence onto the magnetic pitch angle $\varphi_{\rm m}$ in all our models.

(iv) *Corotation radius.* Our dynamo model for NGC 6946 predicts a phase shift between magnetic and preceding optical arm from $\simeq 65^\circ$ to $\simeq 90^\circ$ which is similar to the observed values if we assume a corotation radius of about 10 kpc. This contradicts the investigation by Elmegreen et al. (1992). The effect of

the corotation radius onto the magnetic field may animate further observations in order to get improved data of the velocity field in NGC 6946.

Future investigations should take into account possibly important effects, e.g. the steep rotation curve at inner radii, the true vertical density stratification, and the magnetic feed-back onto the eddy diffusivity (η-quenching) and onto the large-scale gas motion (density waves). New sensitive CO and HI observations should provide improved data on the velocity field, the velocity dispersion and the vertical density distribution of the gas in NGC 6946. Knowledge of the gas density in the magnetic arms requires deep searches for cold gas between the optical arms through CO emission and absorption line observations.

Acknowledgements. R.R. thanks the Deutsche Forschungsgemeinschaft for support (project Ru 488/7). Matthias Ehle is acknowledged for valuable comments to improve the paper.

References

Beck R., Hoernes P., 1996, Nat 379, 47
Beck R., Brandenburg A., Moss D., Shukurov A., Sokoloff D.D., 1996, ARA&A 34, 155
Bloemen J.B.G.M., 1987, ApJ 322, 694
Boulanger F., Viallefond F., 1992, A&A 266, 37
Carignan C., Charbonneau P., Boulanger F., Viallefond F., 1990, A&A 234, 43
Casoli F., 1991, In: Combes F., Casoli F. (eds.) Dynamics of Galaxies and Their Molecular Cloud Distributions. p. 51
Clausset F., Casoli F., Viallefond F., Combes F., 1991, In: Combes F., Casoli F. (eds.) Dynamics of Galaxies and Their Molecular Cloud Distributions. p. 88
Dickey J.M., Lockmann F.J., 1990, ARA&A 28, 215
Ehle M., Beck R., 1993, A&A 273, 45
Elmegreen B.G., Elmegreen D.M., Montenegro L., 1992, Ap. J. Suppl. 79, 37
Elstner D., Meinel R., Rüdiger G., 1990, GAFD 50, 85
Elstner D., Rüdiger G., Schultz M., 1996, A&A 306, 740
Elstner D., Lesch H., von Linden S., Otmianowska-Mazur K., Urbanik M., 1998 Studia geoph. et geod. 42, 373
Fan Z., Lou Y.-Q., 1996, Nat 383, 800
Ferrière K., 1998, A&A 335, 488
Frick P., Beck R., Shukurov A., et al., 1999, MNRAS, submitted
Fröhlich H.-E., Schultz M., 1996, A&A 311, 451
Harnett J.I., Beck R., Buczilowski U.R., 1989, A&A 208, 32
Indrani C., Deshpande A.A., 1998, New Astronomy 4, 33
Kamphuis J., 1993, Ph.D. Thesis, Univ. of Groningen
Kennicutt R.C., 1981, AJ 86, 1847
Kitchatinov L.L., Rüdiger G., 1992, A&A 260, 494
Kitchatinov L.L., Pipin V.V., Rüdiger G., 1994, Astron. Nachr. 315, 157
Krause F., Beck R., 1998, A&A 335, 789
Krause F., Rädler K.-H., 1980, Mean-Field Magnetohydrodynamics and Dynamo Theory. Akademie-Verlag, Berlin
Lou Y.-Q., Fan Z., 1998, ApJ 493, 102
Mestel L., Subramanian K., 1991, MNRAS 248, 677
Moss D., 1997, MNRAS 289, 554
Moss D., 1998, MNRAS 297, 860
Reynolds R.J., 1989, ApJ 339, L29
Rohde R., Elstner D., 1998, A&A 333, 27
Rohde R., Elstner D., Rüdiger G., 1998a, A&A 329, 911
Rohde R., Elstner D., Rüdiger G., 1998b, Studia geoph. et geod. 42, 382
Rüdiger G., Kitchatinov L.L., 1993, A&A 269, 581
Ruzmaikin A.A., Shukurov A., Sokoloff D.D., 1988, Magnetic Fields of Galaxies. Kluwer, Dordrecht
Schreiber E., Schmitt D., 1999, A&A, in press
Shukurov A., 1998, MNRAS 299, L21
Shukurov A., Sokoloff D.D., 1998, Studia geoph. et geod. 42, 391
Sofue Y., 1996, ApJ 458, 120
Subramanian K., Mestel L., 1993, MNRAS 265, 649
Tacconi L.J., Young J.S., 1986, ApJ 308, 600
Tacconi L.J., Young J.S., 1990, ApJ 352, 595